Instant yield stress measurement from falling drop size: The “syringe test”

Anatole Geffrault, Hela Bessaies-Bey, Nicolas Roussel, P. Coussot

Journal of Rheology

Instant yield stress measurement from falling drop size: the "syringe test"

A. Geffrault[1,2], H. Bessaies-Bey[2], N. Roussel[1], P. Coussot[1]

[1] Lab. Navier, Ecole des Ponts, Univ Gustave Eiffel, CNRS, 77420 Marne la Vallée, France

[2] MAST-CPDM, Univ Gustave Eiffel, 77420 Marne la Vallée, France

Abstract: We analyze the different flow regimes of a filament formed by extrusion of a material through a cylindrical die. We deduce that the elongational yield stress of a simple yield stress fluid (i.e., with negligible thixotropy effects) can be determined from the mass of the droplet after filament breakage and an estimation of the critical radius at pinch-off at the solid-liquid regime transition. We demonstrate that such a simple characterization is relevant in a relatively wide range of extrusion velocities, i.e., this velocity slightly affects the drop mass in this range. For the simple yield stress fluids used, Carbopol gel, clay-water paste at different concentrations, emulsion, covering a large range of yield stress values (50 – 1000 Pa), the elongational yield stress appears to be equal to the simple shear yield stress times a factor equal to about $1.5\sqrt{3}$. As a consequence, this simple test may be used to obtain, almost instantaneously and without sophisticated apparatus (a syringe and a balance are sufficient), a good estimate of the shear yield stress of simple yield stress fluids. In that case, the main source of uncertainty (up to about 20%) is the value of the critical radius at the solid-liquid transition. Finally, we review the operating conditions (material properties, extrusion characteristics) for which we can expect this approach to be valid.

1. Introduction

Measuring the yield stress of a yield stress fluid is often considered as a difficult task [1-2]. It is usually considered that it would depend on the geometry or the procedure used [3]. In fact the point is essentially a matter of proper definition and controlled flow characteristics. If the flow geometry effectively allows to get a viscometric flow [4-5], and the procedure effectively allows to distinguish the transition between the solid and the liquid regime, the yield stress should be determined unequivocally as an intrinsic property of the fluid. The problem is more complex when the fluid does not keep its homogeneity during the flow. The situation is also problematic when the fluid is thixotropic [2], since in that case the apparent yield stress depends on the flow history, which means that any rheometrical procedure involving some finite flow duration may lead to a procedure-dependent yield stress value. Finally, for simple yield stress fluids [6-7], i.e. non-thixotropic, reasonable agreement between the flow characteristics under various simple shear flow conditions and the flow curve determined by rheometry (and thus including the yield stress value) were found [8].

Various techniques also exist for estimating the simple shear yield stress from more or less simple and more or less controlled shear flows: slump test, spreading flow, inclined plane flow, squeeze test, object penetration, etc [5]. These techniques essentially provide reasonable estimates of the value of the yield stress in simple shear, which we note here $\sigma_{y,\mathrm{shear}}$ and simply call the yield stress.

On the contrary, relatively few data exist concerning the rheological behavior of yield stress fluid in extensional flow, although such flows are involved in a number of applications For 3D printing of YSF for medical applications [9], ink printing [10], construction materials [11-12], metals for applications in

electronics [13], the extrusion then free surface flow of the filament followed by spreading and stoppage of the yield stress fluid determine the final shape of the object, and elongational flow can play a significant role in the different steps of these processes [14-16].

Most existing works focused on the elongational yield stress ($\sigma_{y,\text{elong.}}$), which we will consider here as corresponding to the yield stress under a simple uniaxial elongational deformation. Note that $\sigma_{y,\text{elong.}}$ is the total critical normal stress applied along the direction of elongation and the second normal stress difference in the extra-stress tensor. First of all, let us remark that one generally assumes that there should exist some proportionality factor between the elongational yield stress and the simple shear yield stress. In this context, the usual reference is the prediction of the "standard" Oldroyd 3D model [17-19], extrapolated from the simple shear Herschel-Bulkley model expression with the help of a Von Mises yield stress criterion, which predicts $\sigma_{y,\text{elong.}} = \xi \sigma_{y,\text{shear}}$ with $\xi = \sqrt{3}$.

Various experimental values were obtained for ξ , say between $\sqrt{3}$ and 3, essentially through experiments consisting to observed the critical conditions at drop formation after extrusion through a die or from extension of a fluid drop between two plates [20-25]. Finally an original approach with the same principle of plate separation but using smooth plates allowing an almost perfect wall slip (i.e. with wall slip yield stress close to zero), and thus a priori a homogenous elongational flow in the whole sample, concluded that the ratio of the elongation yield stress to the shear yield stress is larger (i.e. $\xi = 1.5\sqrt{3}$) than expected from the standard theory [26]. Besides, it was suggested that the pinch-off behavior of yield stress fluids presents nonuniversal trends that should be described with the help of nonlocal rheological models [27]. In parallel, more sophisticated approaches were recently developed either allowing a direct comparison of the detailed flow characteristics of an elongational flow with the predictions of a constitutive equation [28], or the deduction, without preliminary assumption, of the elongational flow curve from the analysis of the detailed characteristics over time of an extruded filament evolving as successive drops [29].

Here we intend to test further the possibility of measuring the elongational yield stress from a simple practical test, as it was already proposed as a simple means for characterizing materials used in additive manufacturing [30]. In that aim we focus on the gravity flow of an extruded filament of yield stress fluid. We start by further analyzing the conditions of transition from solid to liquid regime in the filament. This allows to clearly define the yielding conditions, and thus the normal stress associated with these critical conditions. Using this approach for simple yield stress fluids of different structures and whose yield stress covers a range of more than one decade, we deduce a general law for ξ which appears to be close to $1.5\sqrt{3}$. We can thus define more properly the procedure for estimating the yield stress from this simple technique, which, finally, can also be used as a very simple way to estimate the simple shear yield stress of simple fluids.

2. **Materials and Methods**

2.1 Materials

We used three model yield stress fluids of different structure types, which exhibit negligible thixotropic properties and whose yield stresses are relatively large. We prepared a concentrated direct emulsion from dodecane oil (88% of the total volume) and an aqueous solution containing 3% of TTAB (tetradecyltrimethylammonium bromide), an ionic surfactant (see preparation and characteristics in [29]). We also used kaolin (clay) (*Speswhite, Imerys*) suspensions at different solid volume fractions (here indicated in %) in demineralized water. A homogeneous suspension is rapidly obtained by mixing

the powder and water in a mixer at 150r/min for a few minutes. At last, we used a commercial hair gel (*Vivelle Dop*). Polymer molecules (Carbopol) are present at a few percent concentration in the water solution, thus creating a linked structure that confers it a yield stress fluid behavior.

For each material type the reproducibility and stability of the fluid behavior was confirmed by comparison of flow curve measurements before and after each series of extrusion experiments with a new batch of material.

2.2 Shear rheometry

We characterized the mechanical behavior of the materials by shear rheometry, with a stress controlled *Malvern Kinexus pro+* rheometer equipped with parallel disks geometry of diameter 50 mm with rough surfaces and a gap of 1 mm. As we suspected significant edge effects affecting data with this material, measurements for the gel were carried out with a Couette geometry with serrated wall surfaces, a gap of 4.5 mm, and inner diameter and height of 25 mm and 37.5 mm. To assess the behavior in the liquid regime, we imposed increasing then decreasing stress ramps over 2 min, after a preshear at 10 s^{-1} during 20 s. In the first part of the increasing ramp the material is in its solid regime, but then, i.e. in the liquid regime, the increasing and decreasing stress vs shear rate curves rather well superimpose beyond some critical stress (see Figure 1); the slight remaining differences can be due to some evolution of edge effects. Thus, thixotropic effects are negligible, and we retain the decreasing curve as fully representing the behavior in the liquid regime in steady state (see Figure 1). The validity of this conclusion is proved for the emulsion: the steady state flow points obtained from creep tests indeed superimpose to the decreasing curve (see Figure 1). Under these conditions, the material yield stress is a unique parameter of the material whose value may be estimated from the plateau level in the flow curve. Finally, in the next steps we directly determined the (simple shear) yield stress value of the material as the value of the parameter $\sigma_{y,\text{shear}}$ in the Herschel-Bulkley model fitted to the down ramp flow curve data (see Figure 1), a model which expresses as:

$$\sigma > \sigma_{y,\text{shear}} \;\Rightarrow\; \sigma = \sigma_{y,\text{shear}} + k\dot{\gamma}^{n} \qquad (1)$$

where k and n materials parameters, and σ and $\dot{\gamma}$ respectively the shear stress and shear rate amplitudes. The uncertainty on rheometrical tests, and thus on the rheological parameter values provided, which may be deduced from a repetition of similar tests, can be considered in our case to be about 5%. For the kaolin suspensions at other concentrations the yield stress is directly estimated from the level of the apparent plateau at low shear rates in the decreasing flow curve (see Appendix 1).

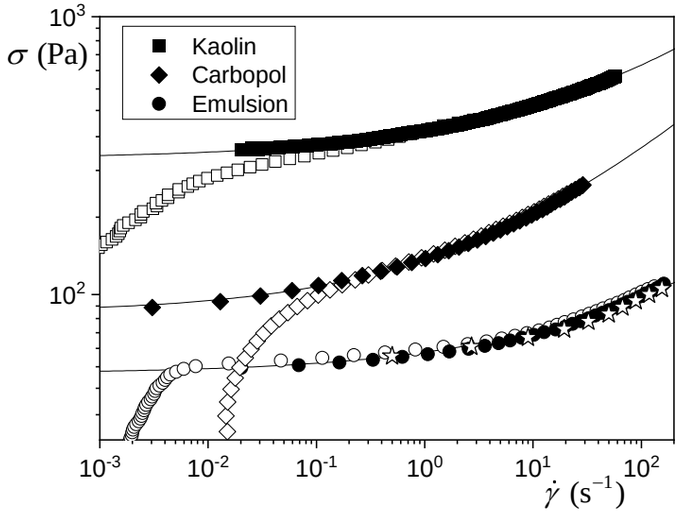

Figure 1: Apparent flow curve of each material type obtained from up and down (stress) ramp test (open symbols for ramp up – filled symbols for ramp down) and steady state flow in the liquid regime during creep tests (stars) for the emulsion. The continuous lines correspond to the Herschel-Bulkley model in simple shear fitted to data (see parameters in Table 1).

Material/parameter	$\sigma_{y,\mathrm{shear}}$ (Pa)	k (Pa s^n)	n
Kaolin suspension (27%)	309	78	0.33
Carbopol gel	86	48	0.36
Emulsion	52	10.8	0.33

Table 1. Parameters of the Herschel-Bulkley model fitted to flow curve data (see Figure 1)

2.3 Set up for extrusion

The setup for extrusion of the pastes is a traction machine (INSTRON) that has been adapted to be used as an extruder (see [29]). The upper part is a piston, which can be moved vertically at a velocity controlled within 0.2%. This piston moves in a 12 cm diameter cylinder, with a nozzle at its bottom. We used three nozzle diameters: 1, 2 and 4 cm. The contact between the piston and the inner cylinder surface is maintained with the help of a seal, which precludes any leakage. The cylinder is initially filled with the material, then the piston is moved at a given velocity which extrudes the material through the nozzle (see Figure 2). The mean velocity of the extrudate could be varied from $0.036\ \mathrm{mm.s^{-1}}$ to $900\ \mathrm{mm.s^{-1}}$.

2.4 Imaging

Each extrusion test is filmed with high resolution (1080*1920) at 60 fps with a Panasonic Lumix FZ82, from the beginning of the exit of the filament from the nozzle to its breakage. The treatment of images allowing to get the apparent diameter all along the filament at different times during extrusion was described previously [29]. Here, we essentially used these data to estimate the volume of each cross-section of the filament, assuming it is perfectly cylindrical and its radius is given from our observations in these videos. Note that the images shown in the present paper to illustrate the filament evolutions were not used for such detailed analysis (i.e. data treatment) of the filament shape.

2.5 Weighing

The filament breakage leads to its separation in successive portions, which we call drops. We measured the drop mass with the help of a balance placed at about 30 cm below the die. Each new drop thus reaches the balance. For such a height no splash was observed with our paste drops. A typical test involves a series of ten or more successive drops. The average drop mass for a given extrusion process could be directly deduced from the final mass divided by the number of drops having reached the balance during this period of time. In addition, in order to control possible fluctuations or evolutions of the drop mass during the test, the evolution in time of the mass on the balance was recorded by a computer. Due to various inertia effects in the system, it is necessary to analyze in details the signal of apparent mass over time to extract some information concerning individual drop mass. We found that under given conditions, after the first drop, the drop mass was stable, with some fluctuations around the mean value which can be considered as the uncertainty.

3. Results and discussion

3.1 Flow regimes and drop formation

Let us examine the mechanisms of drop formation during the extrusion of a yield stress fluid in air. We follow the evolution of the filament shape, from the formation of the previous drop, as a function of the position (X) along its axis from the filament tip (O) (see Figure 2). We consider an extremely slow extrusion. This assumption will in particular make it possible to more clearly distinguish the solid regime from the liquid regime (see below). At the very first time, i.e. just after the separation and fall of the previous drop, we have an inverted cone (see Fig. 2a) which results from the flow associated with the formation of the previous drop. As the material further extrudes, the filament diameter is always first imposed by the die size. We could only observe some swelling at the die exit with the Carbopol gel, which is somewhat viscoelastic [31], but it can be neglected as the corresponding filament diameter increase is in the order of 3%.

Let us now assume for the sake of simplicity that each fluid layer, i.e. situated in a cross-section at some position X , is formed at the exit of the die and then moves downwards while being essentially elongated along the main flow axis. In other words, we assume that at each time the fluid velocity is uniform along a cross-section. Note that this assumption does not mean that shearing is completely absent, as non-diagonal components in the stress tensor can still be significant as soon as the filament diameter varies along X (see [29]).

Under these conditions, the filament section tends to reduce as soon as it moves out of the die, under the action of the weight of material below. However, at a short distance from the die, i.e. in the region between C and B (see Figure 2c), the material is still partially retained by the die. This explains the progressive decrease of the filament diameter just below the die. Beyond some distance the filament shape is not anymore influenced by the die, but just subjected to gravity. We can consider that this occurs when the diameter decreases with X , i.e. in the region BA (see Fig. 2c).

Let us recall that, in this region, as long as the filament is not in contact with the ground, it may be shown from a force balance on the filament portion situated below some cross-section (see [29]), that the average normal stress in this section is equal to the weight (m) of the filament portion per unit cross-section surface:

$$\sigma_{zz} = \frac{mg}{\pi R^2} \tag{2}$$

in which R is the radius of this cross-section. As a consequence, this normal stress, which tends to elongate the sample, increases with the distance from O. Moreover, it rapidly increases when the filament radius decreases. Note that here we use a simplified expression, neglecting inertia effects associated with acceleration (see [29]); these effects result in an additional term in (2), equal to the integral of $a\,\mathrm{d}m$ over the material volume situated below the cross-section under consideration, in which a is the acceleration and $\mathrm{d}m$ the mass of a (cross-sectional) layer (which depends on the current cross-section radius). This term is generally negligible except in the very last times of breakage (see [29]).

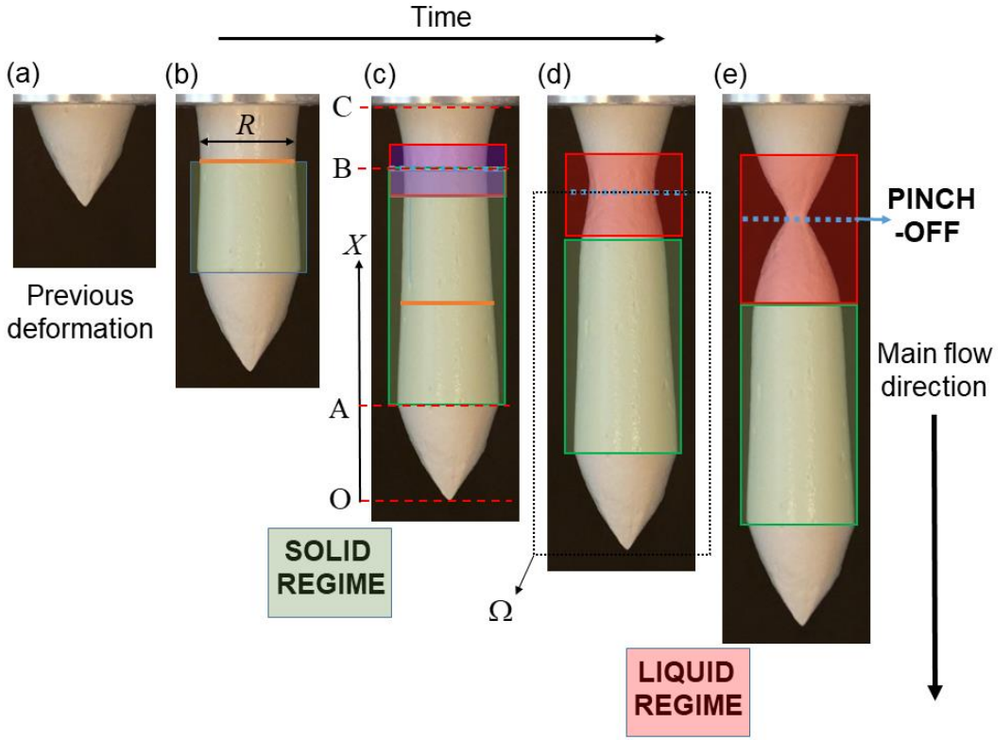

Figure 2: Illustration of the different flow regimes during extrusion of a filament of yield stress fluid (here Kaolin, 27%, die diameter 2 cm) under gravity, just after the fall of the previous drop. Successive images of the filament: (a) Cone formed during previous drop fall, (b) and (c) Development of a region deformed in the solid regime, (d) and (e) Development of a region in the liquid regime and flow in this region.

Thus, during extrusion, a layer formed at the die exit elongates progressively as it moves downwards; then it reaches its minimum value in B, where the influence of the die is negligible. In that case, if the weight of material below the fluid layer is sufficiently small, this fluid layer, while it goes on advancing downwards, will keep its radius constant. This is illustrated in Figure 2 by the orange mark which moved downwards from (b) to (c). In this situation the material has undergone the maximum possible deformation in the solid regime under the action of a normal stress σ_{zz}, so that it will a priori not deform anymore. We effectively observe that the deformation of a layer is generally fixed from its passage through B: the filament region between A and B negligibly deforms during the rest of the process (see Fig. 2b,c). In this regime the material has typically undergone a limited elastoplastic deformation (see [29, 31-32]). Finally, the normal stress increasing with the distance from O, the resulting deformation increases with X, which explains the conical shape of the sample in the solid region AB. Nevertheless, note that for some materials, at the approach of the yield stress, some residual viscous flow may be observed in the solid regime [31], which can lead to some slight further deformation.

Since the filament shape around the pinch-off region is essentially cylindrical the deformation it undergoes is essentially a simple uniaxial elongation (see [29, 32]). Since afterwards, as above described, during further motion, each such layer essentially keeps its size, we deduce that the region AB corresponds to the solid regime of the material under these simple extensional conditions. More precisely, the deformation (from the initial value, i.e. the die radius R_0) associated with each local $R(X)$ value and assuming a pure elongation, corresponds to the final deformation the material reached in elongation when subjected to a normal stress $\sigma_{zz}(X)$. The filament shape in region AB can thus be used to deduce the constitutive equation of the material in elongation.

This solid regime takes place only over a limited distance. Since the normal stress increases with X and with $1/R$, there exists a time for which the layer in B is subjected to a stress equal to the yield stress in elongational flow. At that time, the deformation starts to increase beyond the critical deformation reached for a stress just below the yield stress. This reduces the filament radius in this region, which further increases the stress beyond the yield stress value, potentially inducing a faster flow. However, it would not be possible to have a liquid flow restricted to an infinitely thin layer still in contact with undeformed solid regions. The flow in the liquid regime in this layer in B probably induces a large increase of the stress around this layer, inducing a flow of some regions of finite thickness above and below this layer (see Fig. 2d). This results in much larger deformation than expected in the solid regime, in a region of finite size situated around B, which we refer to as the liquid flow region.

Note that during this process capillary effects remain negligible. Indeed, let us recall the main lines o the basic approach proposed to compare the order of magnitude of viscous effects under slow flow conditions (i.e. when the stress is in the order of the yield stress) and surface tension effects. Then we compare the work associated with the main stress (i.e. the normal stress) during some elementary strain in a layer of initial thickness h and radius R, i.e. $-(\pi R^2 h)2\sigma_{zz}dR/R$, to the surface energy variation resulting from this deformation, i.e. $\gamma\,\mathrm{d}(2\pi Rh) = -2\pi\gamma h dR$ (where γ is the surface tension of the fluid, close to that of the interstitial liquid). We find that surface tension effects will be negligible if $\sigma_{zz}R >> \gamma$. Moreover, it is valuable to remark that in the pinch off region, the left side term of this equation increases when the radius decreases, since the normal stress approximately increases with $1/R^2$ (assuming a constant weight). It follows that it is sufficient to have $\sigma_{c,\mathrm{elong.}}R_0 >> \gamma$ (with R_0 the initial radius), i.e. negligible surface tension effects, at the very beginning of the flow, for surface tension effects to be negligible all along the separation process.

The study of the flow characteristics in the liquid region has been the object of our previous work [29], showing that the apparent deformation of the filament may be used to deduce the behavior of the material in an extensional flow. More precisely, the elongational rate of strain ($\dot{\varepsilon}$) is deduced from the evolution of the filament radius over time ($\dot{\varepsilon} = 2dR/Rdt$) and the normal stress from (1) in addition taking into account the acceleration term. Finally, the flow curve for extensional flow is essentially deduced from the data in the pinch-off region, i.e. $\dot{\varepsilon}$ and σ_{zz} are computed at the position of minimum R, where non-diagonal components in the stress and strain rate tensor are negligible (see [29]). The results of this approach for the Carbopol gel are presented in Figure 3, and the (corrected) results previously obtained for the emulsion and a kaolin suspension are recalled in Figure 10 in the Appendix. For the two latter materials the shape of the constitutive equation in extensional flow is close to the prediction from the standard 3D expression derived from the Herschel-Bulkley model (see [29]), but for the Carbopol a strong difference appears at high strain rate (see Figure 3). This difference is likely due to the presence of polymers in the material, which tend to induce an increase of the elongational viscosity when the strain rate increases, an effect (now in terms of shear viscosity) which is much more limited in simple shear. For all materials the yield stress in elongation is significantly larger than the prediction from the von Mises criterion used in the 3D model.

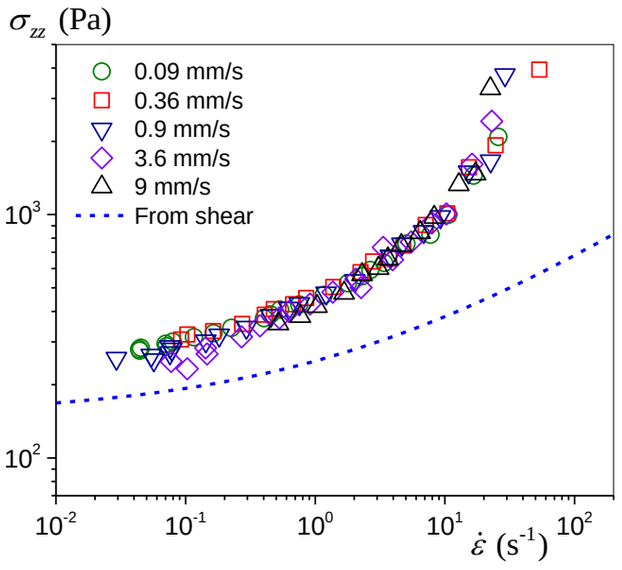

Figure 3: Flow curves in elongational flow for the Carbopol gel for different extrusion velocities. The blue dotted line corresponds to the prediction of the standard 3D Herschel-Bulkley model in pure elongational flow (see Appendix 3). Note that this standard expression is based on the use of the rheological parameters in simple shear; we use for that the values determined in simple shear tests (see Table 1).

Pinch-off and drop mass

According to the above analysis we expect that the yielding will occur when the stress in the pinch-off layer is equal to the elongational yield stress. Here we study how the filament shape can be predicted or interpreted in terms of yield stress of the material. In regards to this aim, if the layer of material in which yielding occurs remains at the pinch-off point until breakage, then the material amount situated below the pinch-off remains equal to the mass associated with the critical weight inducing the yield stress. As a consequence, the mass of the drop finally obtained after breakage will provide the value of the elongational yield stress.

In this context it is useful to look at the evolutions of the volume of filament below the pinch-off (point B) during all the process. From videos of the filament formation, we estimated the apparent volume (Ω) of material in the region situated below B (see Figure 4). In all cases we observe a regime during which the volume below pinch-off increases widely while the filament radius at the pinch-off point slowly decreases, followed by a regime in which this volume remains constant while the radius at pinch-off strongly decreases. The former regime corresponds to the formation of the solid region as above described, i.e. as long as the normal stress at pinch-off is below the yield stress. The latter regime corresponds to the liquid regime above described, when the yield stress at the pinch-off has been reached. Our assumption here is that as soon as the yield stress has been reached the flow will start around the pinch-off point, and since the extrusion velocity is extremely small, this flow will rapidly lead to the separation of the filament in two parts, with the volume below the initial pinch-off region remaining constant.

Although it is easy to distinguish the two regimes it is not so easy to precisely determine the point of transition between them. Looking more precisely at the data it appears that in the liquid regime the volume still slightly varies, an effect which could come from some uncertainty in the data analysis or could be due to the complex deformations of the filament in the liquid regime. As a consequence, here

we will arbitrarily consider that the critical radius for which the solid to liquid transition occurs is situated in the range corresponding to a volume between 10% and 5% smaller than the volume extrapolated by fitting a straight line (dashed line in Figure 4) along the data in the second regime. This leads to ranges for the critical radius shown by blue rectangles in Figure 4. In that case, the resulting uncertainty on the value of the critical radius can then be up to 10%, which induces an uncertainty on the corresponding critical stress of about 20%.

Note that the transition between the two regimes was specifically studied in a previous work [21]. In that case the approach consisted to follow the evolution of the apparent strain rate in the pinch-off region, to determine the time, and thus the tensile stress or the critical radius, for which the strain rate variations significantly change (from slow to fast). This makes it possible to identify a point of transition with a limited uncertainty. However, we cannot clearly relate this transition to the physical mechanisms of solid-liquid transition we describe above. As a consequence, especially in view of determining the yield stress from the drop mass, we think more appropriate to rely on a criterion consistent with both the standard characteristics of the solid-liquid transition for yield stress fluid and the prediction of the final volume of the drop.

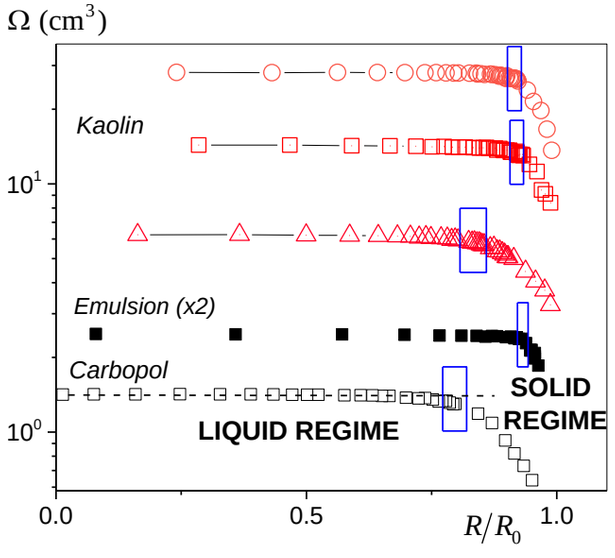

Figure 4: Volume below pinch-off during the drop formation as a function of the pinch-off to die radius ratio for the different materials (extrusion velocity**:** 0.36 mm/s, except for Kaolin 31%: 0.9 mm/s): (from top to bottom) kaolin, 31, 27 and 23%; Emulsion (drop volume multiplied by 2); Carbopol gel. The blue rectangles represent the ranges of radii in which the transition between the two regimes can be considered, from which we estimate the value of R_c. The dashed line is fitted to data at small radius.

Impact of extrusion velocity on the drop mass

So far, we considered theoretically a vanishing extrusion velocity, and experimentally the lowest velocity permitted by our set up. In view of using this approach in practice for determining the elongational yield stress it is critical to be aware of the impact of the extrusion velocity on the characteristics of the process.

Let us first consider the problem from a theoretical point of view. For a simple yield stress fluid whose behavior can be represented in terms of a stress equal to a constant value (i.e. the yield stress) plus a

term increasing with the flow rate and tending to zero when the flow rate tending to zero, the material flows at an increasing rate when the stress increases above the yield stress. As a consequence, for a finite extrusion velocity, from the time the yield stress has been reached at the pinch-off, the filament has time to significantly further advance and a larger normal stress is reached in a section above the first pinch-off section. The material may then tend to flow in its liquid regime at a higher rate in this section than in the initial pinch-off section. Under these conditions the radius may soon reach a smaller value in this section than in the first yielding section, and finally the filament breakage will occur above the initial pinch-off section. This effect leads to an increase of the drop mass after breakage with the extrusion velocity, since the breakage will occur later for higher extrusion velocity.

Looking at the videos by comparing the filament aspect at the same moment of extrusion for different velocities we effectively see that the drop size increases with the extrusion velocity (see Figures 5-6). For all materials there is a range of extrusion velocities in which the drop size remains rather constant. For the emulsion and the kaolin suspensions this range is rather large, it extends over several decades, typically from 0.1 to about 20 mm/s (see Figures 5a and 6a,b). However, for the kaolin there is also a slight increase of the drop size from the lowest velocities. For the Carbopol the range of almost constant drop size only extends up to about 2 mm/s (see Figure 6c). Note that for this material the effective drop breakage is delayed by the development of a long filament. Finally, with a slight further increase of the extrusion velocity the filament remains continuous, i.e. no drop appears to form (see Figure 6).

In order to have a better view of the phenomena occurring during the transition from a single drop of constant volume to a continuous jet of approximately uniform radius, we show in Figure 5b the pictures of the emulsion drops in a narrower range, i.e. 20 – 360 mm/s. Remarkably, for a velocity larger than about 120 mm/s, the next drop, of roughly similar size, starts to develop in the filament region above the previous drop while the latter is not detached yet. This phenomenon may appear in contradiction with the description of the drop formation as a result of the mass of material situated below the pinch-off region, since below the upper pinch-off region the mass is about twice the critical mass associated with the elongational yield stress. In fact, this likely comes from the fact that the acceleration terms (see below and [29]) play a major role in that case, thus relieving a part of the stress.

Finally the jet becomes continuous when the time of separation of the drops is too large compared to the extrusion velocity, so that the successive drops which tend to form, do not have time to break (see 360 mm/s in Figure 5b). Note that the characteristic time of breakage can in theory be computed since we have identified that a pure elongational flow occurs in the pinch off region and we know the constitutive equation of each material in elongation. In that aim one has to compute the strain rate at each step of the radius decrease leading to filament breakage. However, this time essentially depends on the flow conditions in the slowest stage, i.e. just after the transition from the solid to the liquid regime. This period can hardly be appreciated as the flow rate is in theory infinitely low when the stress tends to the yield stress, and in practice we cannot decide precisely when this transition occurs (see above). Future works, in the spirit of the analysis of the evolution of filaments of simple liquids in one or several droplets [33], might complete this basic analysis, and in particular describe the specific flow instabilities leading to these complex patterns with yield stress fluids.

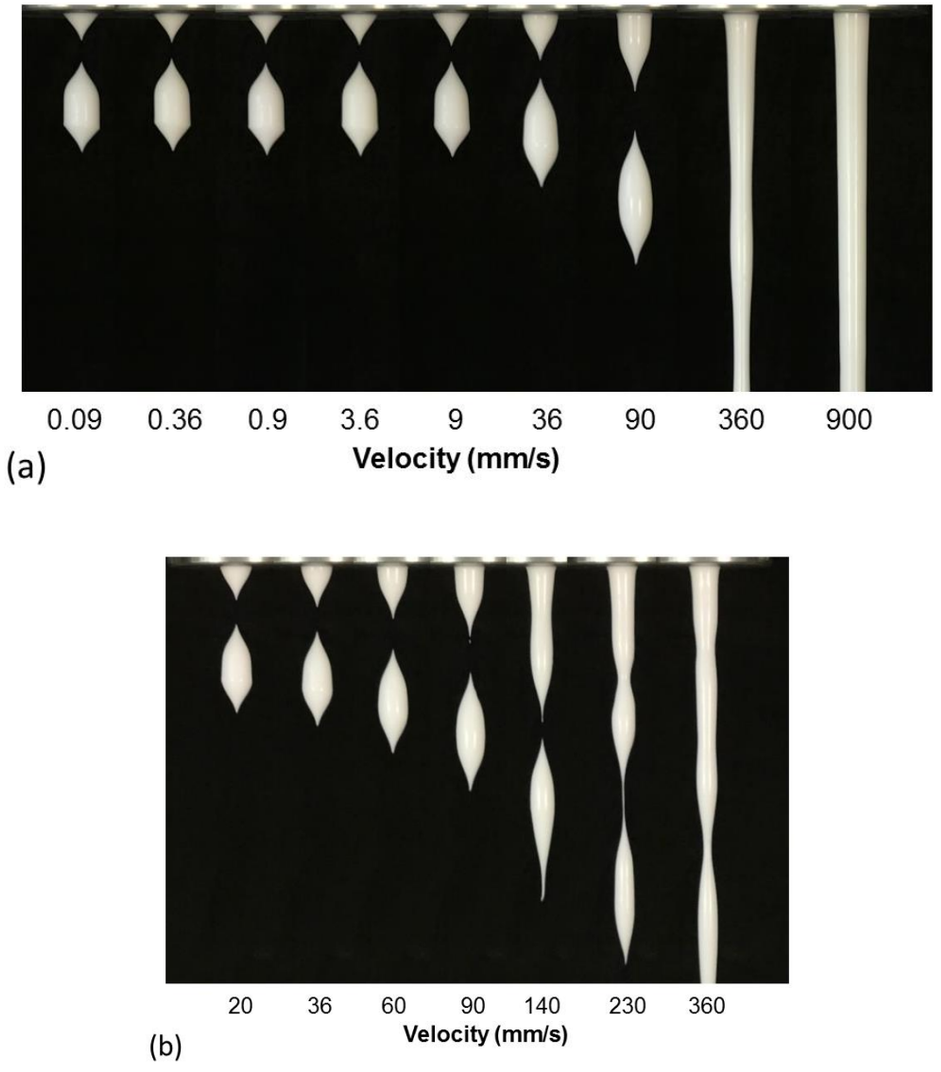

Figure 5: Images of the filament for different extrusion velocities for the emulsion: (a) in the full range of velocities tested, (b) in a narrower range of velocities around the regime transition. The images presented here correspond to the first image after filament breakage when a breakage occurs, and to the image for which the filament is the thinner in the other cases (largest velocities).

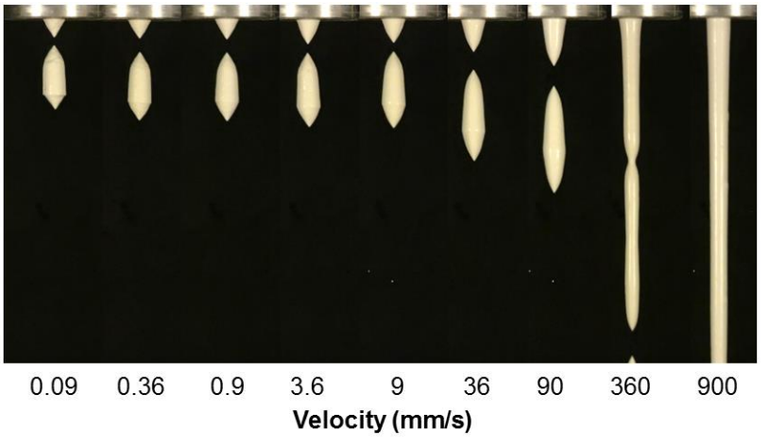

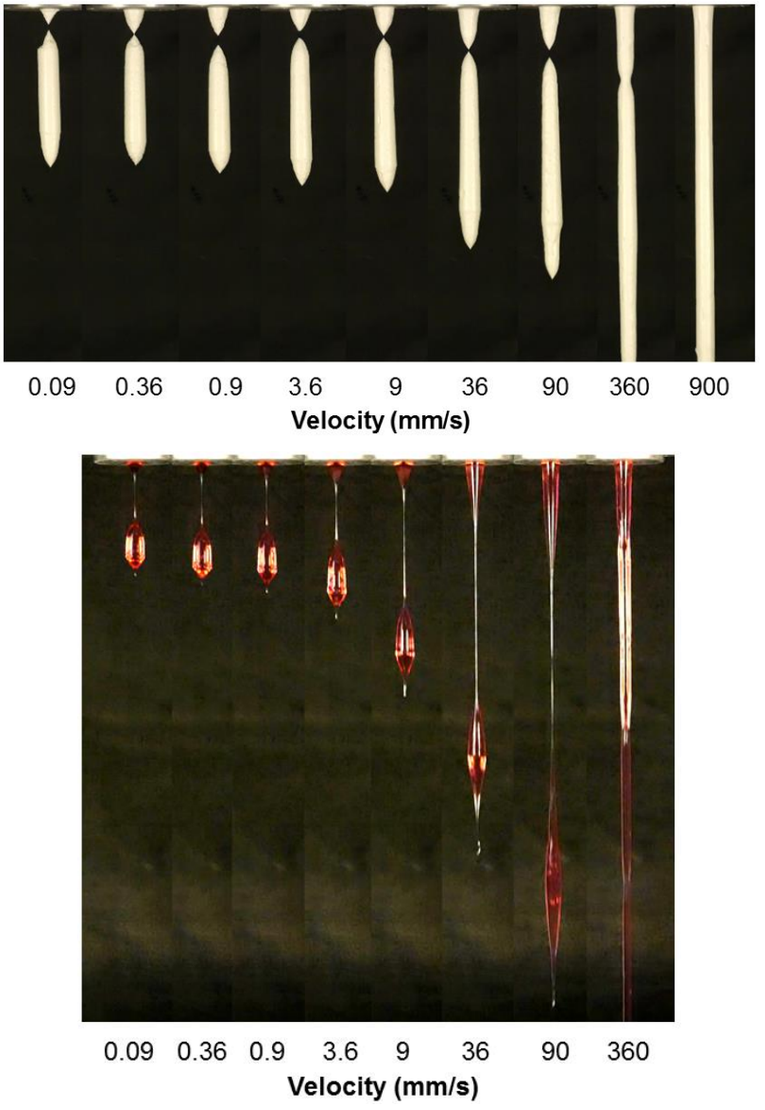

Figure 6: Images of the filament for different extrusion velocities for kaolin suspensions ((a) 23%, (b) 29%) and Carbopol gel (c).

In order to quantify these variations with the extrusion velocity (V) we measured the drop mass (m_d) in these different experiments (see Materials and Methods) (see Figure 7). Generally the drop mass only slightly fluctuates around the mean value, the maximum fluctuation is considered as the uncertainty, and is represented by error bars in Figure 7. Note that the values deduced from volume estimations from videos are consistent with these data, which confirms the validity of the successive above analyses of the processes from the observation of the filament shape evolution. We obviously observe the same tendencies as from the series of pictures above: a long plateau for the emulsion, a slight increase for kaolin, and a short plateau then strong increase for the Carbopol.

Remarkably, there is some similarity between the shape of these curves and the flow curves of the materials obtained from simple shear rheometrical tests (see Figure 1): the flow curves of the kaolin suspensions and the emulsion are much flatter than that of the Carbopol which increases more rapidly with the shear rate.

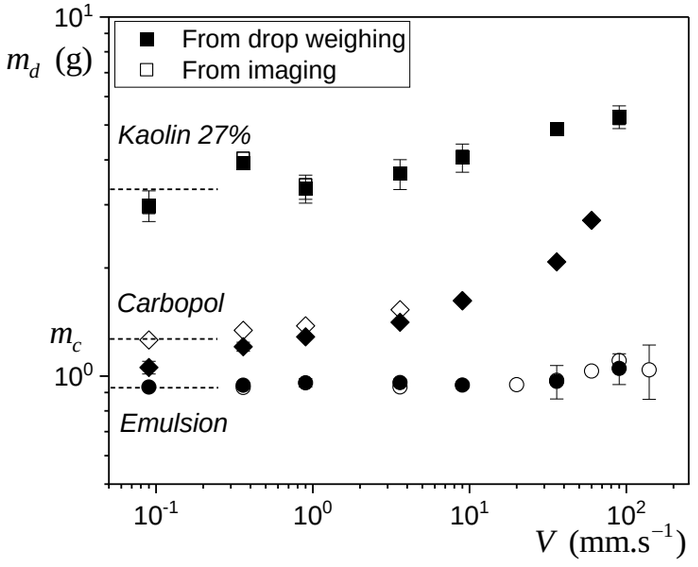

Figure 7: Drop mass as a function of the extrusion velocity for the different materials.

Elongational yield stress

With this knowledge of the filament flow and breakage mechanisms we now have the means to relevantly analyze the data of drop mass in terms of elongational yield stress. From the tests carried out at different extrusion velocities we retain the mass value (m_c) associated with the plateau in the drop mass vs velocity (see Figure 7). On another side we use the curves of apparent drop volumes as a function of radius at pinch-off as shown in Figure 4, to estimate the value of R_c corresponding to the transition from the solid to the liquid regime in the pinch-off layer. The elongational yield stress is then determined from

$$\sigma_{c,\text{elong.}} = \frac{m_c g}{\pi R_c^{\,2}} \tag{3}$$

Let us remark that since the square power of R_c is involved in this expression taking into account the effective critical radius at the regime transition is essential. As abovementioned the uncertainty on its exact value is at the origin of an uncertainty up to 10% on the yield stress determination.

We can now plot the elongation yield stress value for the different materials, i.e. emulsion, Carbopol and kaolin suspension at different concentrations, in the same diagram (see Figure 8) as a function of the yield stress ($\sigma_{c,\text{shear}}$) estimated from the simple shear flow curve. It appears that all data fall along a straight line, i.e. $\sigma_{c,\text{elong.}}$ is simply proportional to $\sigma_{c,\text{shear}}$. More precisely we have

$$\sigma_{c,\text{elong.}} \approx 1.5\sqrt{3}\sigma_{c,\text{shear}} \tag{4}$$

This result is in agreement with the observations during extension of similar simple yield stress fluids between two smooth plates allowing perfect wall slip [34]. Note however that this value of 1.5 is just an approximation (see Figure 8) and has no theoretical explanation for now.

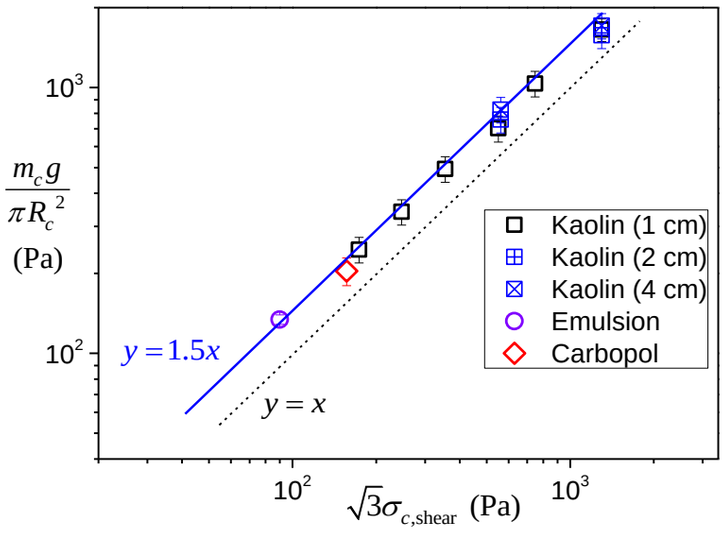

Figure 8 : Drop mass per unit exit cross-section, i.e. the elongational yield stress according to our interpretation (see text and equation (2)), for different material types or concentrations (for kaolin) as a function of the shear yield stress times $\sqrt{3}$.

Conclusion

From the analysis of the different flow regimes of a filament formed by extrusion of a material through a cylindrical die we were able to deduce the elongational yield stress of simple yield stress fluids. It is obtained from the mass of the droplet after filament breakage and an estimation of the critical radius at pinch-off at the solid-liquid regime transition. This elongational yield stress appears to be equal to the simple shear yield stress times a factor equal to about 1.5 $\sqrt{3}$. Since it is in agreement with previous measurements using extension between smooth surfaces ensuring a perfect slip [34], this result seems robust. However, there lacks some theoretical explanation of this result which is in contradiction with the prediction from the standard description of the constitutive equation for a Herschel-Bulkley fluid. In this context it is in particular remarkable that we obtain a similar factor for materials of very different fluid microstructures.

These observations provide a simple means to measure the elongational yield stress. In that aim one just needs a balance and a syringe with a die radius R_0 of the order of 0.5 cm. The mass of a series of droplets extruded by the syringe at a sufficiently low extrusion velocity, say of the order of a few millimeters per second, should be measured. Then the elongational yield stress will be estimated from equation (3). Since there is no simple means to estimate R_c we suggest to refer to our results for different material types and use $R_c = 0.8R_0$ for gels and $R_c = 0.9R_0$ for other materials. Note that the uncertainty on the exact value of is likely the main source of uncertainty for the yield stress determination with this technique. This uncertainty was estimated to be smaller than 10% in our context, i.e. with the help of detailed observations of the filament characteristics. The uncertainy may be larger, say up to 20%, in the absence of such observations, e.g. when only using drop mass measurements and the abovementioned values.

If we admit the generality of the result concerning the relationship between the elongational yield stress and the shear yield stress for simple yield stress fluids, we can even conclude that this simple technique could be directly used to estimate the shear yield stress of a material.

"Let us finally review the operating conditions of this technique in terms of material properties and extrusion characteristics:

- **Material type**. The technique is specifically fitted to yield stress fluids. However, the technique is directly relevant for sufficiently simple yield stress fluids. For thixotropic yield stress fluids, which in general exhibit a yield stress increasing with the time of rest the approach should be completed by considering the yielding condition evolution during extrusion and filament flow. If one can consider that the material goes out of the die in a given state the separation will a priori start for longer drop length when decreasing the extrusion velocity, since the material has more time to restructure before reaching the liquid regime in the pinch-off region. As soon as the liquid regime has been reached, we expect a fast separation, as for simple yield stress fluids, since the normal stress increases for decreasing filament diameter. Thus, the apparent elongational yield stress should increase for decreasing velocity, and the technique will provide the yield stress value as a function of the time of rest (or, more precisely, the time spent in the solid regime) since its exit from the die. This time is roughly equal to the ratio of the length of the filament between the die exit and the pinch-off point to the extrusion velocity. Note that this length before separation seems to remain in the order of the die diameter. Finally, an increase of drop size for decreasing velocity might be the hallmark of a thixotropic behavior.
  We could also expect some limitations of the technique for materials with specific structure, such as suspensions containing polymers, which can exhibit large elongational viscosities, or with granular pastes, in which some jamming of solid particles may form during elongation. In both cases one would expect more marked effects for decreasing filament diameters. However, this should not impact the present approach aimed at determining the elongational yield stress since in any case, as soon as the material has reached the liquid regime the drop will eventually separate. However, for such materials, the simple relationship found between the elongational yield stress and the simple shear yield stress might not be valid anymore. Moreover, with such materials the range of extrusion velocities for which the approach is valid might be reduced, since if the viscosity for small filament diameter is larger, the time needed for separation will be larger and the range of velocities for which drops have time to form will reduce. Nevertheless, in this range, elongational yield stress measurements from drop size are relevant as long as the continuum assumption is valid, i.e. for sufficiently large filament diameter to particle size ratio.
- **Yield stress range**. In the present work we tested materials with yield stress ranging from 50 to 1000 Pa. It might be possible to use the technique with higher yield stress values but it is difficult to test this possibility as for such materials simple shear flows may easily be affected by shear-banding or rupture, as they are closer to pure plastic solids than to fluids. Within the frame of our study the lower limit of yield stress was imposed by the smallest die diameter, i.e. 1 cm, so that capillary effects are negligible. Moreover, following our criterion (see text) it would theoretically be possible to carry out tests while keeping negligible capillary effects and with a yield stress going down to zero, by increasing the die diameter. However, in that case the Rayleigh-Taylor instability may occur, leading to spontaneous gravity flow of the fluid.
- **Extrusion characteristics**. As seen above, the die diameter must be sufficiently large for surface tension effects to be negligible. Conversely, for high yield stress materials it is possible to use very small die diameters.
  As for the extrusion velocity it must remain in the range for which the drops have a constant size. This range somewhat depends on the material behavior, for example on the importance of the second term in the Herschel-Bulkley representation. The typical range of velocities in which we can expect a constant drop size is 0-10 mm/s, so that one can recommend to carry

out experiments at a velocity of 1 mm/s or smaller to ensure getting the proper drop size, which can be directly used for determining the elongational yield stress.

Appendix 1: **Rheological data for kaolin suspensions at different concentrations.**

Here we present the full data (decreasing shear rate ramp) for kaolin suspensions at different concentrations (see Figure 9).

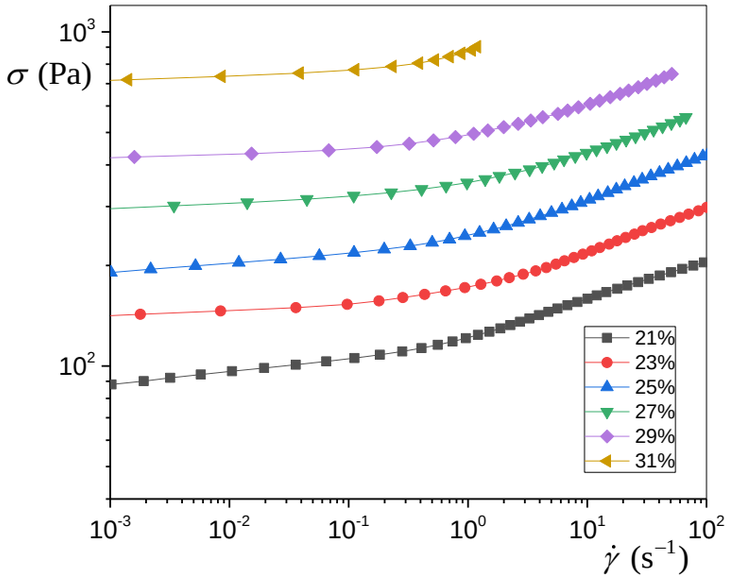

Figure 9: Flow curves in the decreasing ramp for kaolin suspensions at different concentrations.

Appendix 2: Flow curves in elongational flow as deduced from filament extrusion and flow.

Here we show the data (see Figures 10 a,b) obtained in a previous work by analyzing the normal stress and the deformation at the pinch off during the extrusion of a filament of emulsion and a kaolin paste [JOR]. We take this opportunity to proceed to a correction of these data. Indeed, due to a confusion in the software between the (normal) stress and extra-stress tensor, a coefficient 2/3 was erroneously applied to the stress values, leading to underestimate the effective normal stress. Here we present the corrected data. Note that since this factor was applied in any case in the analysis this does not affect the shape of the flow curve data.

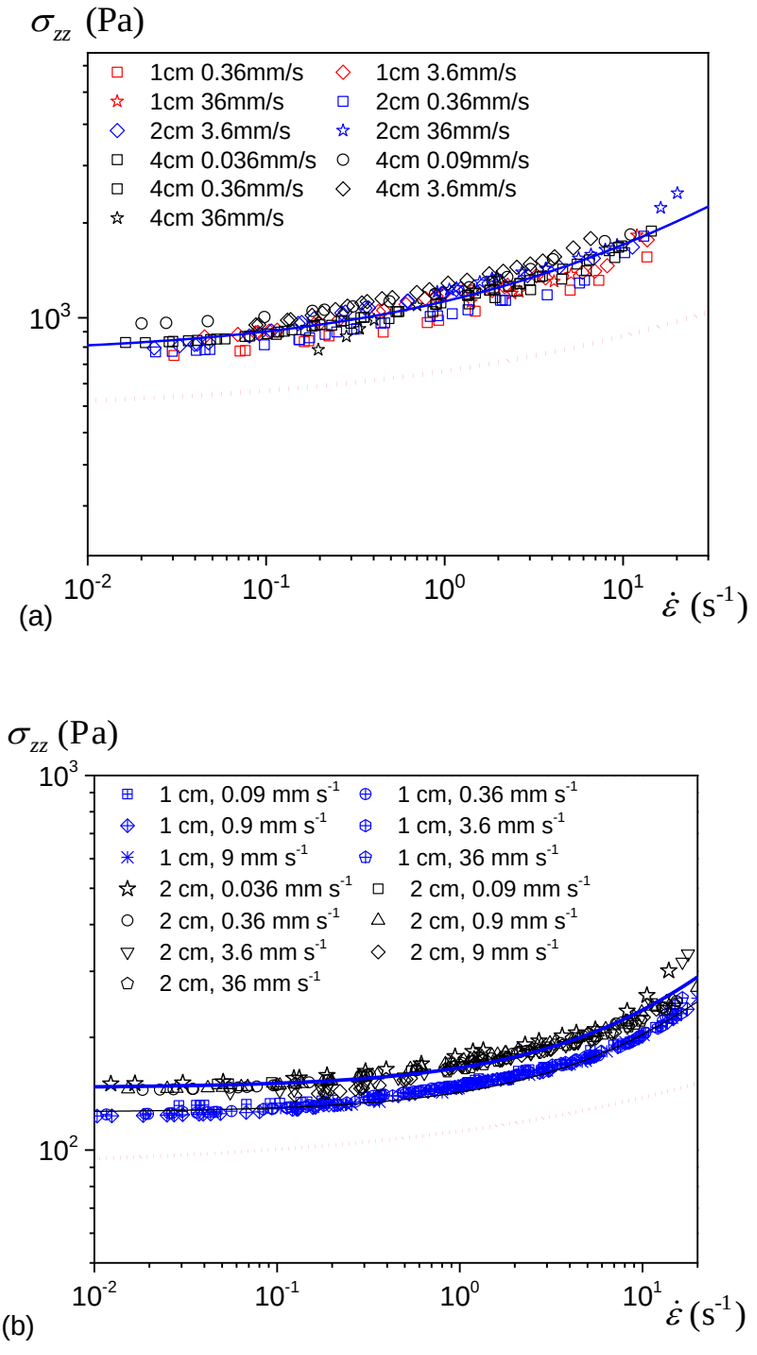

Figure 10: Flow curves in elongational flow for the kaolin suspension (a) and the emulsion (b) under different conditions (see legend). The red dotted lines corresponds to the expression derived from the standard 3D Herschel-Bulkley model in pure elongational flow (i.e. equation (6)) using the rheological parameters determined in simple shear (see Table 1). The thick continuous blue lines correspond to the best fit of a Herschel-Bulkley model for the elongation flow (i.e. equation 6), with parameters: $\sigma_{c,\text{shear}} = 448$ Pa, $k = 157$ Pa s^n and $n = 0.4$ for the kaolin, and $\sigma_{c,\text{shear}} = 85$ Pa, $k = 7.6$ Pa s^n and $n = 0.67$ for the emulsion. For the emulsion this fit was done on the data for a 2 cm

diameter; the thin black line is this best fit with the stress times a factor 0.86 (i.e. $\sigma_{c,\text{shear}} = 73.1$ Pa , $k = 6.5$ Pa s^n and $n = 0.67$).

Appendix 3: Constitutive equation in simple uniaxial elongation as deduced from the standard 3D expression for a Herschel-Bulkley fluid.

The 3D form of this constitutive equation has been the subject of discussions but the simplest form initially proposed by Oldroyd [17] is as follows:

$$\sqrt{T_{II}} > \sigma_{c,\text{shear}} \;\Rightarrow\; \boldsymbol{\Sigma} = -p\mathbf{I} + \sigma_{c,\text{shear}} \frac{\mathbf{D}}{\sqrt{D_{II}}} + \left(\frac{2^n k}{(D_{II})^{(1-n)/2}} \right) \mathbf{D} \qquad (5)$$

in which $\boldsymbol{\Sigma}$ is the stress tensor, $\mathbf{I}$ the identity tensor, $T_{II} = \frac{1}{2}\text{tr}\mathbf{T}^2$ and $D_{II} = \frac{1}{2}\text{tr}\mathbf{D}^2$ are the second invariants of $\mathbf{T}$ and $\mathbf{D}$, where $\mathbf{T}$ is the extra-stress tensor defined as $\boldsymbol{\Sigma}(Z,t) = -p\mathbf{I} + \mathbf{T}$ with $\text{tr}\,\mathbf{T} = 0$.

For a purely elongational flow, we have $D_{II} = \frac{3}{4}\dot{\varepsilon}^2$ and $T_{II} = \frac{\sigma_{zz}^{\ 2}}{3}$, where σ_{zz} is the diagonal stress component along the main axis of elongation, so that the constitutive equation in the liquid regime writes:

$$|\sigma_{zz}| > \sqrt{3}\sigma_{c,\text{shear}} \Rightarrow \sigma_{zz} = \sqrt{3}\left[\tau_c + k\left|\sqrt{3}\dot{\varepsilon}\right|^n \right] \qquad (6)$$

References

[1] Nguyen, D.Q., D.V. Boger, "Yield stress measurement for concentrated suspensions", J. Rheology, 27, 321 (1983)

[2] Moller, P.C.F., J. Mewis, D. Bonn, "Yield stress and thixotropy: on the difficulty of measuring yield stresses in practice", Soft Matter, 2, 274 (2006)

[3] Dinkgreve, M., J. Paredes, M.M. Denn, D. Bonn, "On different ways of measuring "the" yield stress", J. Non-Newt. Fluid Mech., 238, 233 (2016)

[4] Coleman B.D., H., Markowitz, and W. Noll, *Viscometric flows of non-Newtonian Fluids* (Springer Verlag, Berlin, 1966)

[5] Coussot P., *Rheometry of pastes, suspensions and granular materials* (Wiley, New York, 2005)

[6] Ovarlez, G., S. Cohen-Addad, K. Krishan, J. Goyon, P. Coussot, "On the existence of a simple yield stress fluid behavior", *J. Non-Newt. Fluid Mech*., 193, 68-79 (2013)

[7] Balmforth, N.J., I.A. Frigaard, G. Ovarlez, "Yielding to stress: recent developments in viscoplastic fluid mechanics", Annual Review of Fluid Mechanics, 46, 121-146 (2014)

[8] Coussot, P. "Yield stress fluid flows: a review of experimental data", *Journal of Non-Newtonian Fluid Mechanics* 211, 31–49 (2014)

[9] Townsend, J. M., E. C. Beck, S. H. Gehrke, C. J. Berkland, M. S. Detamore, "Flow behavior prior to crosslinking: the need for precursor rheology for placement of hydrogels in medical applications and for 3D bioprinting", Prog. Polym. Sci., **91**, 126-140 (2019)

[10] M'Barki A., L. Bocquet, A. Stevenson, « Linking rheology and printability for dense and strong ceramics by direct ink writing », Scientific Reports, **7**, 6017 (2017)

[11] Jeong H., S.-J. Han, S.-H. Choi, Y. J. Lee, S. T. Yi, K. S. Kim, "Rheological property criteria for buildable 3D printing concrete", Materials, **12**, 657 (2019)

[12] Mechtcherine V., F. P. Bos, A. Perrot, W. R. Leal da Silva, V. N. Nerella, S. Fataei, R. J. M. Wolfs, M. Sonebi, N. Roussel, « Extrusion-based additive manufacturing with cement-based materials – Production steps, processes, and their underlying physics : a review », Cement and Concrete Research, **132**, 106037 (2020)

[13] Daalkhaijav U., O. D. Yirmibesoglu, S. Walker, Y. Menguc, "Rheological Modification of Liquid Metal for Additive Manufacturing of Stretchable Electronics", Adv. Mat. Technol, **3**, 1700351 (2018)

[14] Tiwari M. K., A. V. Bazilevsky, A. L. Yarin, C. M. Megaridis, "Elongational and shear rheology of carbon nanotube suspensions", Rheol. Acta, **48**, 597-609 (2009)

[15] Mackay, M. E., "The importance of rheological behavior in the additive manufacturing technique material extrusion", J. Rheol., **62**, 1549 (2018)

[16] Nelson A. Z., K. S. Schweizer, B. M. Rauzan, R. G. Nuzzo, J. Vermant, R. H. Ewoldt, "Designing and transforming yield-stress fluids", Current Opinion in Solid State and Materials Science, **23**, 100758 (2019)

[17] Oldroyd J. G., "A rational formulation of the equations of plastic flow for a Bingham solid", Proc. Cambridge Philosophical Society, **43**, 100-105 (1947)

[18] Hohenemser K., W. Prager, "Über die ansätze der mechanik isotroper kontinua », Zeitschrift für Angewandte Mathematik und Mechanik, 12, 216-226 (1932)

[19] Coussot, P., S.A. Rogers, "Oldroyd's model and the foundation of modern rheology of yield stress fluids", J. Non-Newt. Fluid Mech., 295, 104604 (2021)

[20] Niedzwiedz K., H. Buggisch, N. Willenbacher, "Extensional rheology of concentrated emulsions as probed by capillary breakup elongational rheometry (CaBER)", *Rheol. Acta*, 49, 1103 (2010)

[21] German G., V. Bertola, "Formation of viscoplastic drops by capillary breakup", *Phys. Fluids*, 22, 033101 (2010)

[22] Martinie L., H. Buggisch, N. Willenbacher, "Apparent elongational yield stress of soft matter", *J. Rheol.*, **57**, 627 (2013)

[23] Sadek S. H., H.H. Najafabadi, F. J. Galindo-Rosales, "Capillary Breakup Extension ElectroRheometry (CaBEER)", Journal of Rheology, 64, 43-54 (2020)

[24] Sadek S. H., H.H. Najafabadi, F. J. Galindo-Rosales, "Capillary breakup extension magnetorheometry", Journal of Rheology, 64, 55-65 (2020)

[25] Boujlel J., P. Coussot, "Measuring the surface tension of yield stress fluids", *Soft Matter*, 9, 5898 (2013)

[26] Zhang X., O. Fadoul, E. Lorenceau, P. Coussot, "Yielding and flow of soft-jammed systems in elongation", Phys. Rev. Lett., 120, 048001 (2018)

[27] Louvet N., D. Bonn, H. Kellay, "Nonuniversality in the Pinch-Off of Yield Stress Fluids: Role of Nonlocal Rheology", *Phys. Rev. Lett*., 113, 218302 (2014)

[28] Varchanis S., S. J. Haward, C. C. Hopkins, A. Syrakos, A. Q. Shen, Y. Dimakopoulos, J. Tsamopoulos, "Transition between solid and liquid state of yield-stress fluids under purely extensional deformations", PNAS, 117, 12611-12617 (2020)

[29] Geffrault, A., H. Bessaies-Bey, N. Roussel, P. Coussot, "Extensional gravity-rheometry (EGR) for yield stress fluids", J. Rheology, 65, 887-901 (2021)

[30] Ducoulombier, N., R. Mesnil, P. Carneau, L. Demont, H. Bessaies-Bey, J.F. Caron, N. Roussel, « The « Slugs-test » for extrusion-based additive manufacturing : Protocol, analysis and practical limits », Cement and concrete Composites, 121, 104074 (2021)

[31] Coussot, P., H. Tabuteau, X. Chateau, L. Tocquer, and G. Ovarlez, "Aging and solid or liquid behavior in pastes", J. Rheol., 50, 975-994 (2006)

[32] N'gouamba, E., J. Goyon, P. Coussot, "Elastoplastic behavior of yield stress fluids", Phys. Rev. Fluids, 4, 123301 (2019)

[33] Planchette, C., F. Marangon, W.K. Hsiao, G. Brenn, "Breakup of asymetric liquid ligaments", Phys. Rev. Fluids, 4, 124004 (2019)

[34] Zhang, X., O. Fadoul, E. Lorenceau, P. Coussot, "Yielding and flow of soft-jammed systems in elongation", Physical Review Letters, 120, 048001 (2018)

Journal of Rheology

PLEASE CITE THIS ARTICLE AS DOI: 10.1122/8.0000557

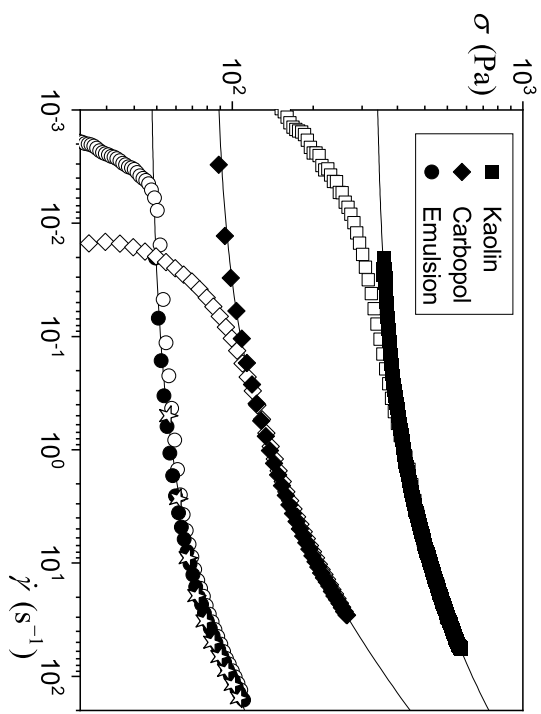

Journal of Rheology

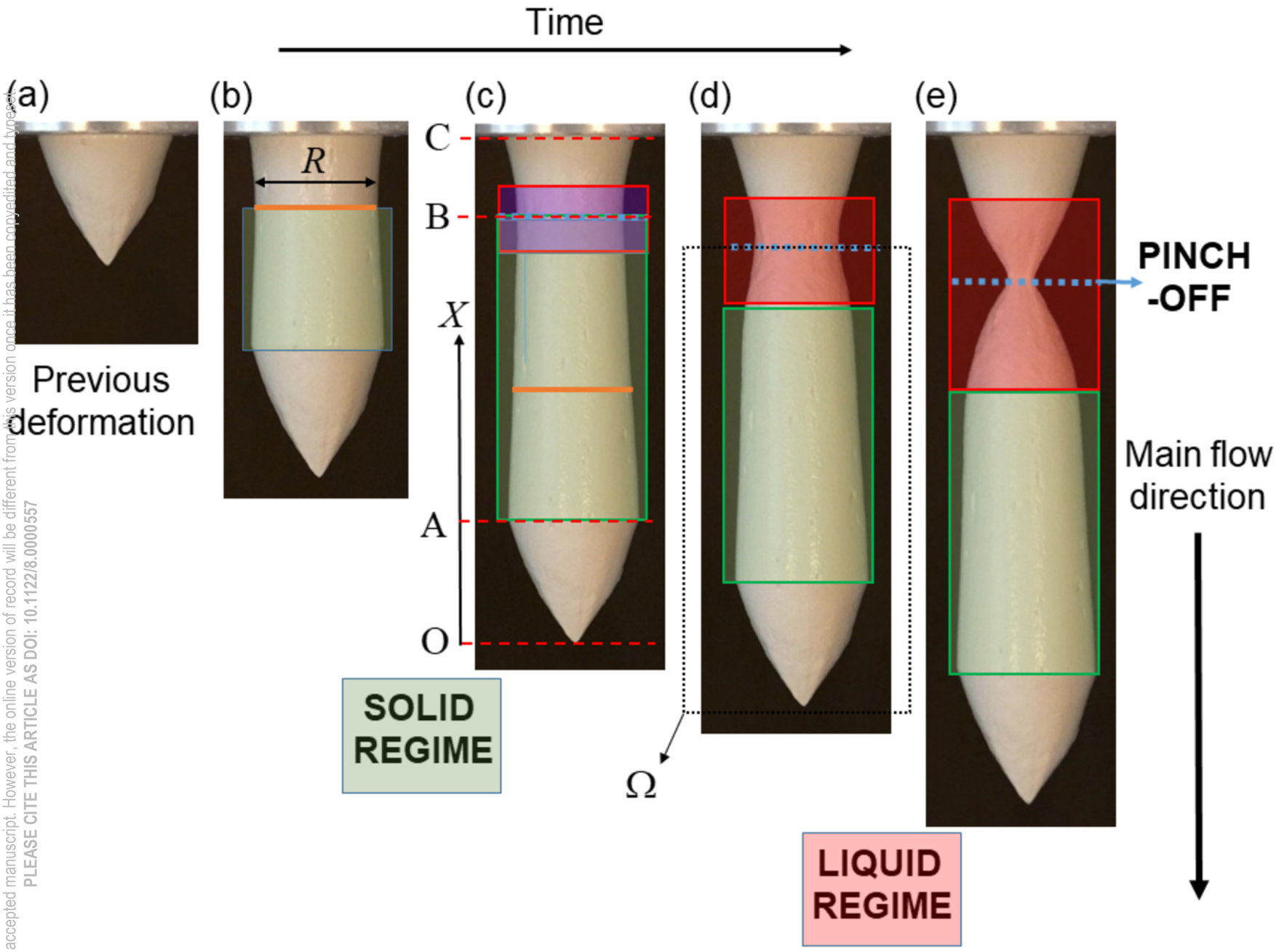

πάντα ῥεῖ

Journal of Rheology

ACCEPTED MANUSCRIPT

PLEASE CITE THIS ARTICLE AS DOI: 10.1122/8.0000557

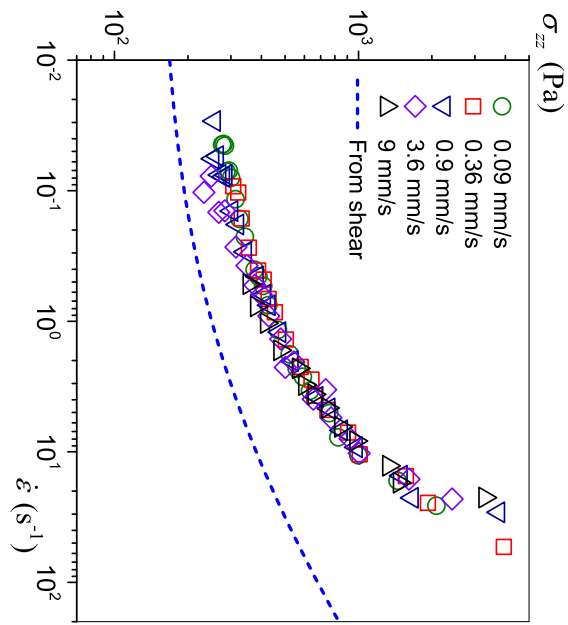

πάντα ῥεῖ

Journal of Rheology

ACCEPTED MANUSCRIPT

PLEASE CITE THIS ARTICLE AS DOI: 10.1122/8.0000557

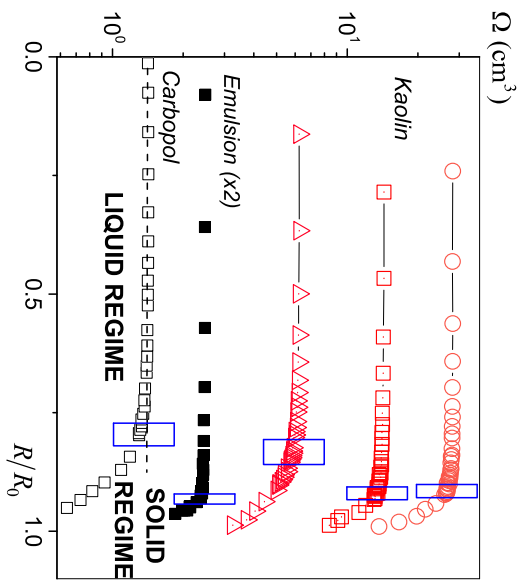

πάντα ῥεῖ
Journal of Rheology ACCEPTED MANUSCRIPT

PLEASE CITE THIS ARTICLE AS DOI: 10.1122/8.0000557

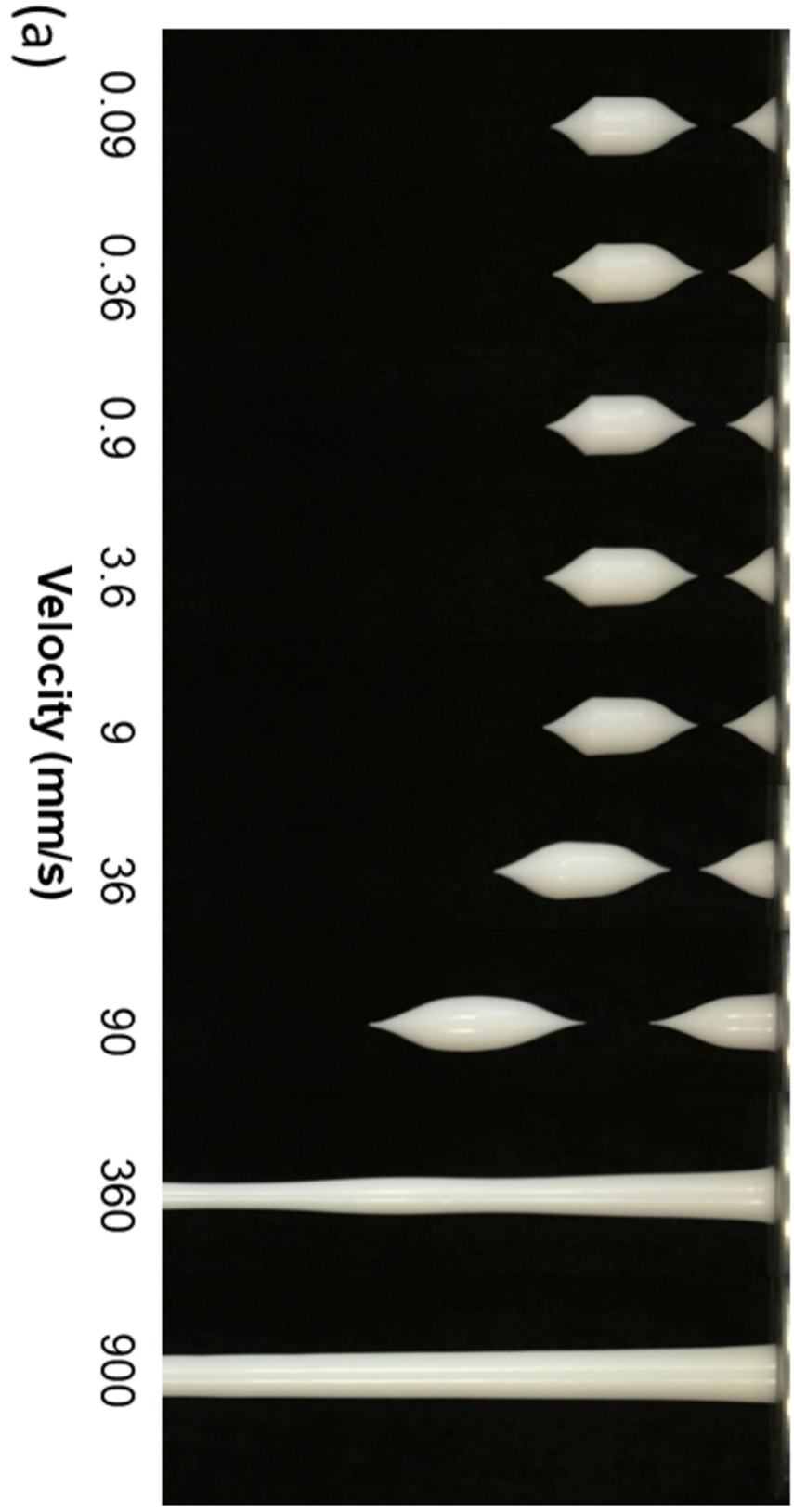

Journal of Rheology ACCEPTED MANUSCRIPT

PLEASE CITE THIS ARTICLE AS DOI: 10.1122/8.0000557

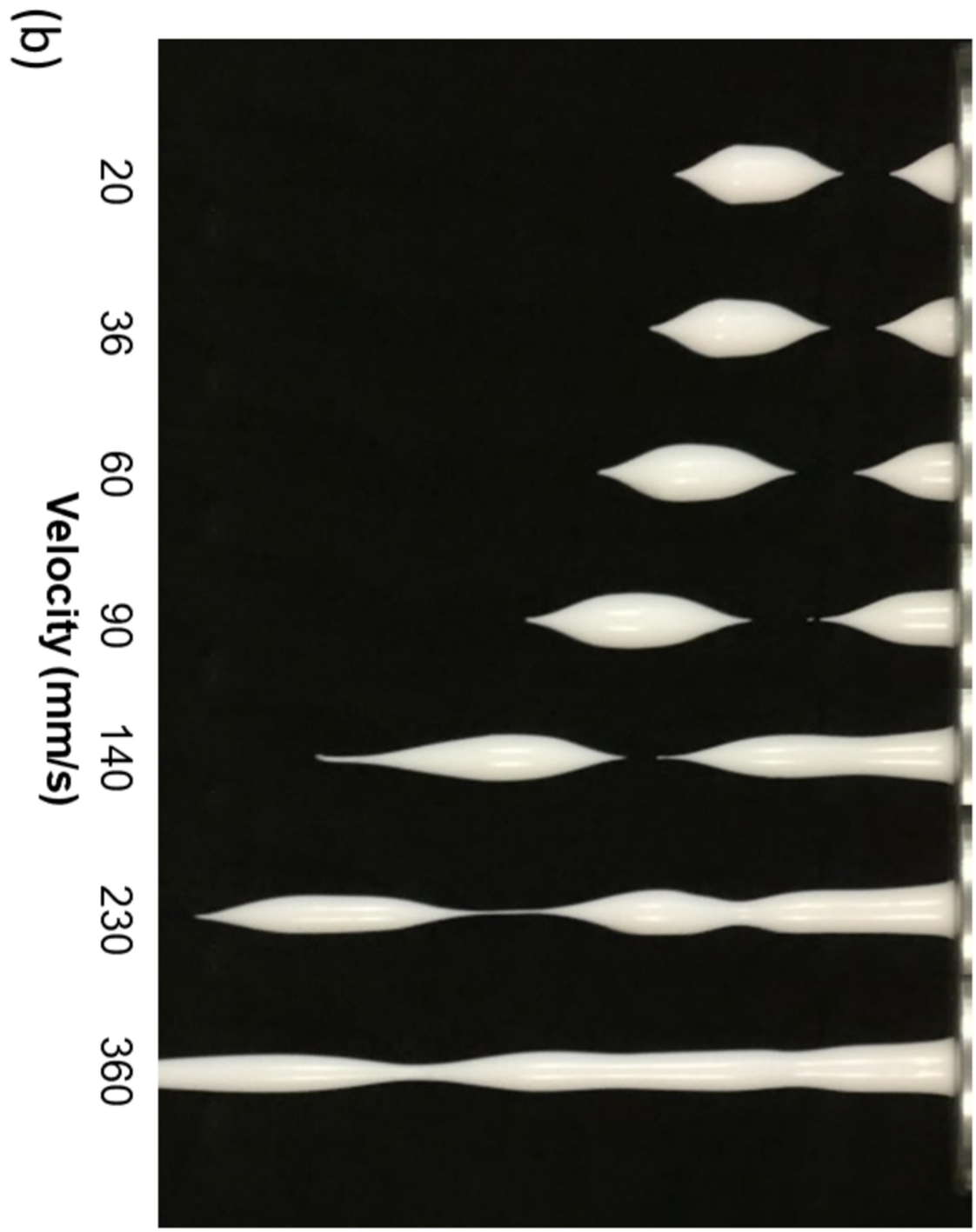

Journal of Rheology ACCEPTED MANUSCRIPT

PLEASE CITE THIS ARTICLE AS DOI: 10.1122/8.0000557

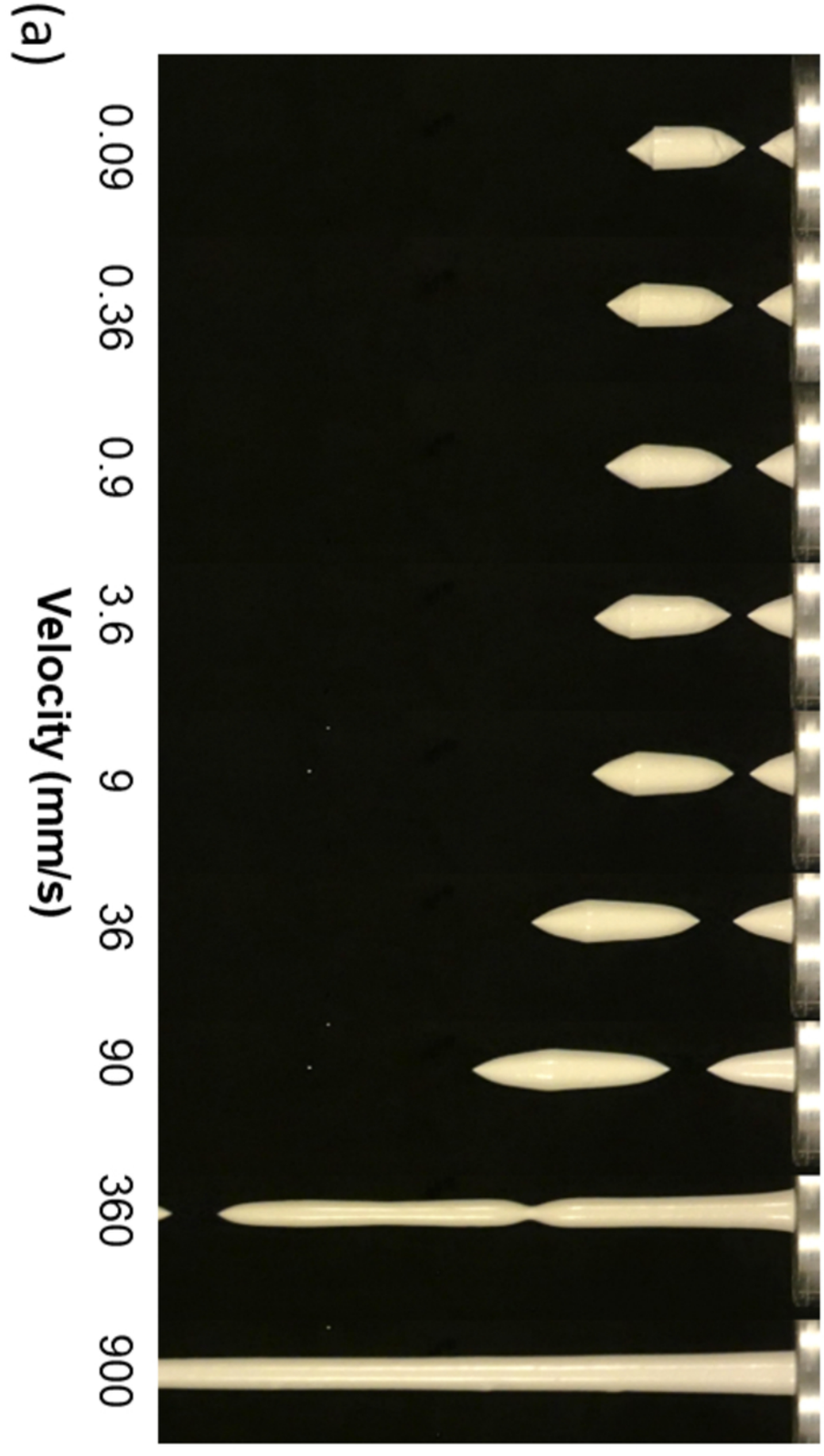

Journal of Rheology ACCEPTED MANUSCRIPT

This is the author's peer reviewed, accepted manuscript. However, the online version of record will be different from this version once it has been copyedited and typeset.
PLEASE CITE THIS ARTICLE AS DOI: 10.1122/8.0000557

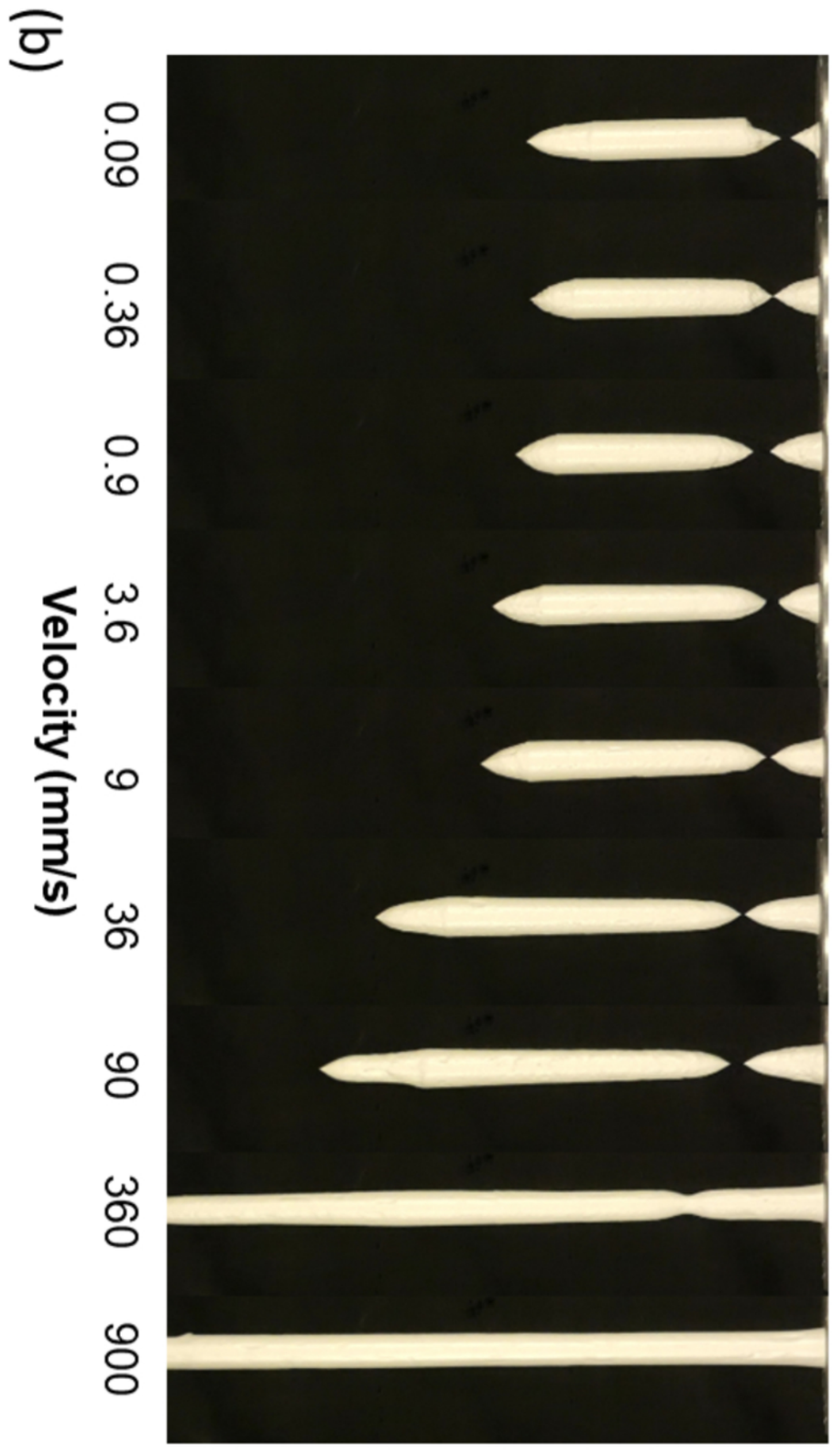

Journal of Rheology ACCEPTED MANUSCRIPT

PLEASE CITE THIS ARTICLE AS DOI: 10.1122/8.0000557

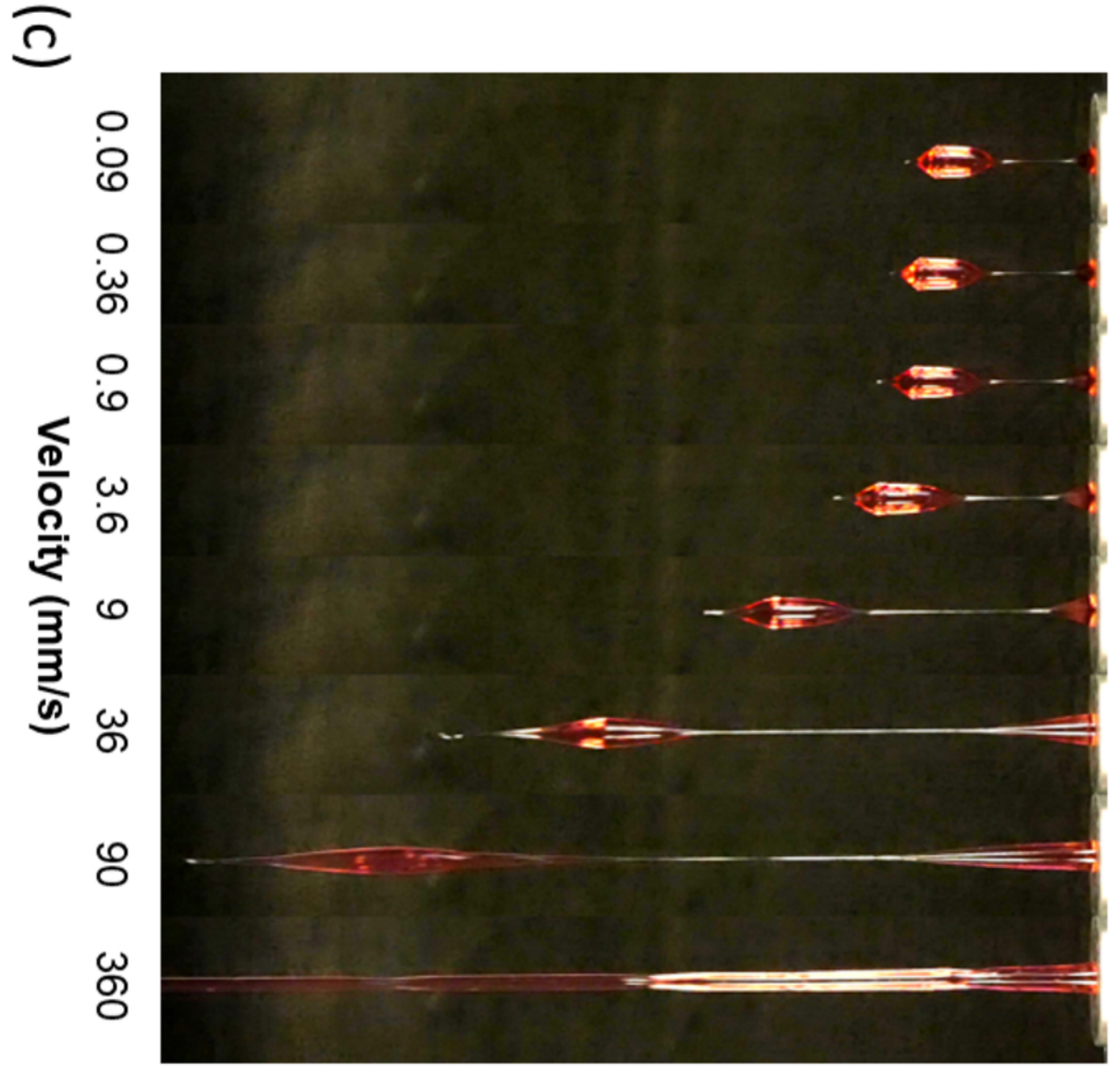

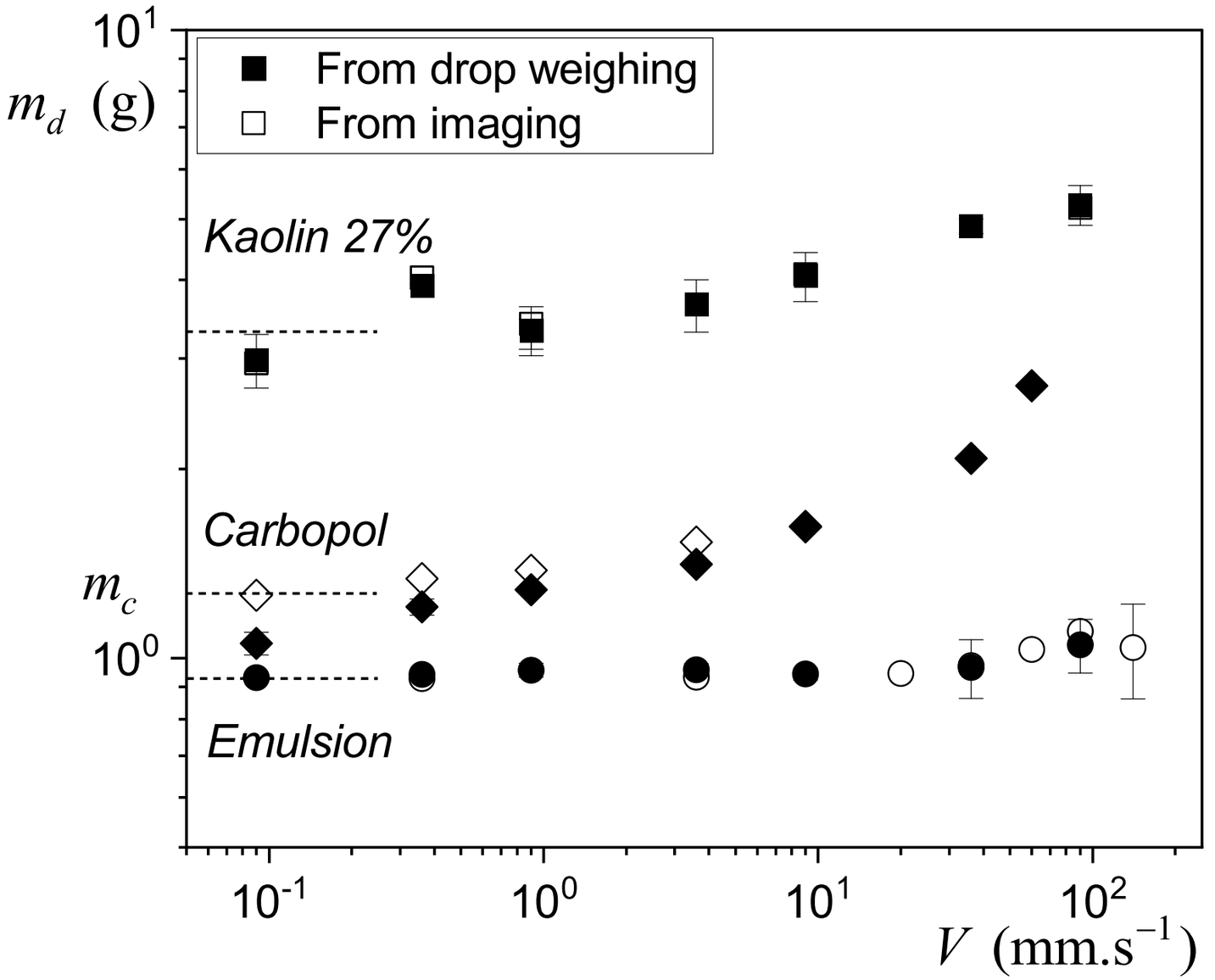

πάντα ῥεῖ

Journal of Rheology

ACCEPTED MANUSCRIPT

PLEASE CITE THIS ARTICLE AS DOI: 10.1122/8.0000557

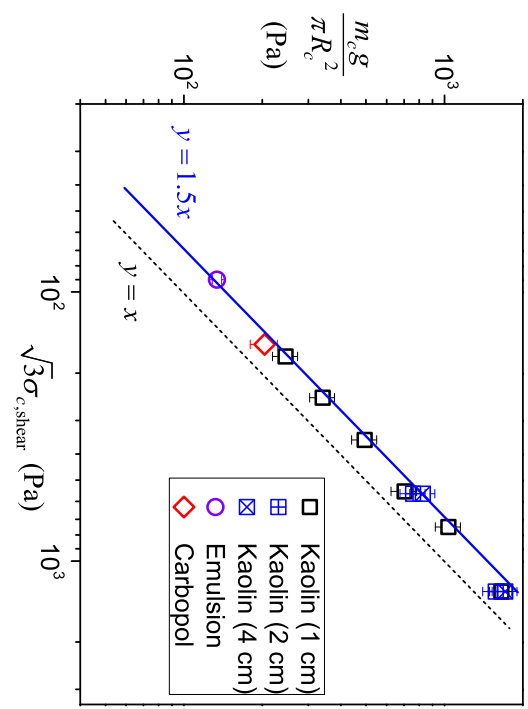

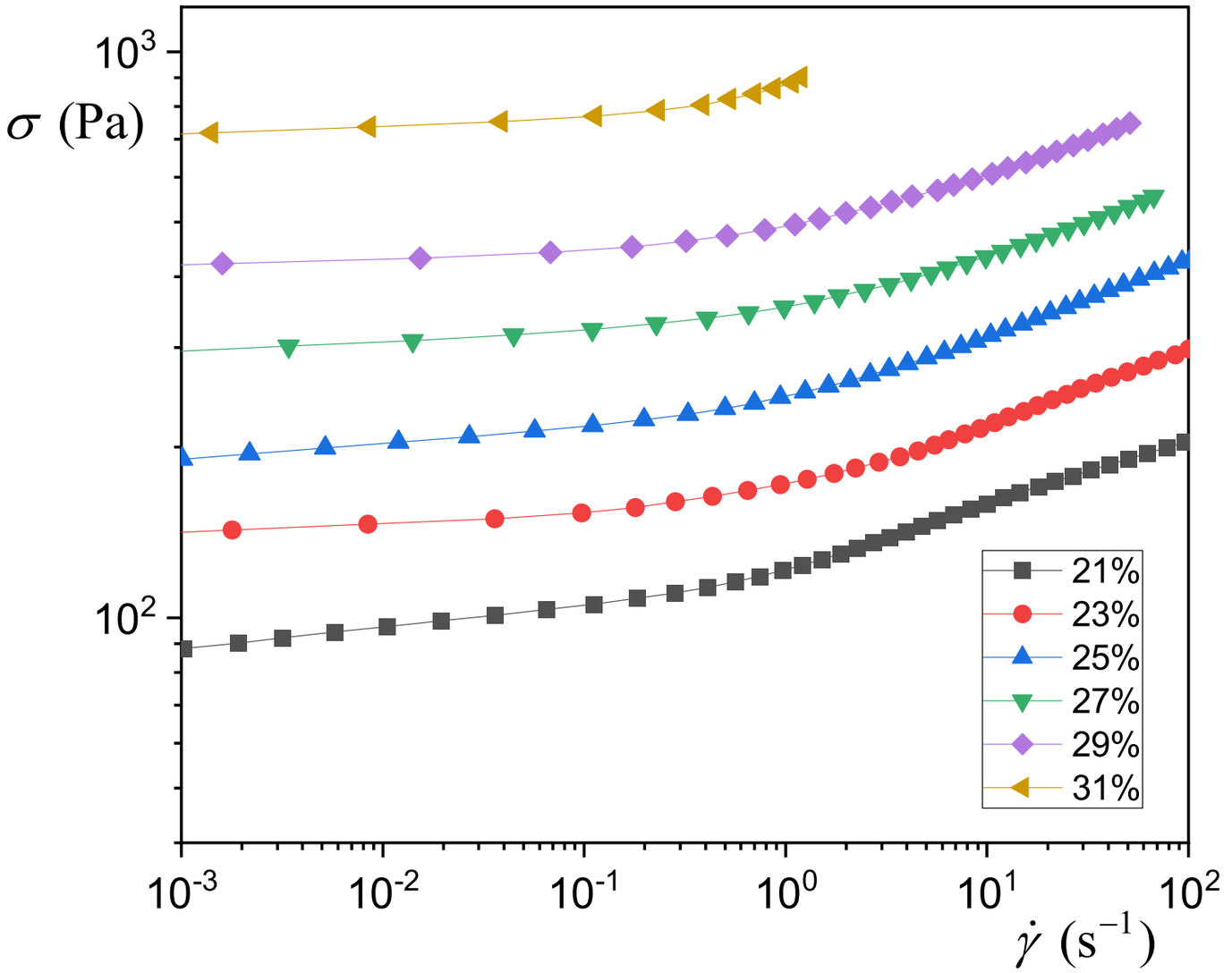

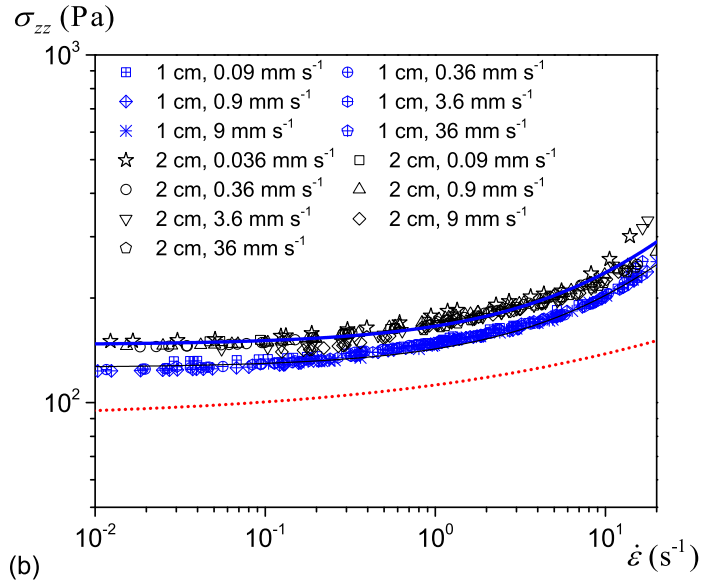

(b)